Structure
Article

Structure of the Kti11/Kti13 Heterodimer and Its Double Role in Modifications of tRNA and Eukaryotic Elongation Factor 2

Sebastian Glatt,[1,7] Rene Zabel,[2,7] Ivana Vonkova,[1] Amit Kumar,[3] Daili J. Netz,[4] Antonio J. Pierik,[4,6] Vladimir Rybin,[1] Roland Lill,[4,5] Anne-Claude Gavin,[1] Jochen Balbach,[3] Karin D. Breunig,[2,*] and Christoph W. Müller[1,*]
[1]Structural and Computational Biology Unit, European Molecular Biology Laboratory, Meyerhofstraße 1, 69117 Heidelberg, Germany
[2]Martin-Luther-Universität Halle-Wittenberg, Institut für Biologie, Weinbergweg 10, 06120 Halle (Saale), Germany
[3]Martin-Luther-Universität Halle-Wittenberg, Institut für Physik, Betty-Heimann-Straße 7, 06120 Halle (Saale), Germany
[4]Institut für Zytobiologie, Philipps-Universität Marburg, Robert-Koch-Straße 6, 35037 Marburg, Germany
[5]LOEWE Zentrum für Synthetische Mikrobiologie SynMikro, Hans-Meerwein-Straße, 35043 Marburg, Germany
[6]Present address: Faculty of Chemistry, University of Kaiserslautern, Erwin-Schrödinger-Straße 54, 67663 Kaiserslautern, Germany
[7]Co-first author
*Correspondence: karin.breunig@genetik.uni-halle.de (K.D.B.), cmueller@embl.de (C.W.M.)
http://dx.doi.org/10.1016/j.str.2014.11.008

SUMMARY

The small, highly conserved Kti11 alias Dph3 protein encoded by the *Kluyveromyces lactis k*iller *t*oxin *i*nsensitive gene *KTI11/DPH3* is involved in the diphthamide modification of eukaryotic elongation factor 2 and, together with Kti13, in Elongator-dependent tRNA wobble base modifications, thereby affecting the speed and accuracy of protein biosynthesis through two distinct mechanisms. We have solved the crystal structures of *Saccharomyces cerevisiae* Kti13 and the Kti11/Kti13 heterodimer at 2.4 and 2.9 Å resolution, respectively, and validated interacting residues through mutational analysis in vitro and in vivo. We show that metal coordination by Kti11 and its heterodimerization with Kti13 are essential for both translational control mechanisms. Our structural and functional analyses identify Kti13 as an additional component of the diphthamide modification pathway and provide insight into the molecular mechanisms that allow the Kti11/Kti13 heterodimer to coregulate two consecutive steps in ribosomal protein synthesis.

INTRODUCTION

Novel regulatory mechanisms of the translation process involving synonymous codon variants but also tRNA modifications have recently gained particular attention (Cannarozzi et al., 2010; Laxman et al., 2013; Novoa et al., 2012; Tuller et al., 2010). Modifications of uridines in the wobble position of tRNA anticodons have been shown to influence ribosomal A-site binding and translation rates of specific proteins (Bauer et al., 2012; Rezgui et al., 2013). Thiolation at the wobble position was recently described in yeast as a sensor for sulfur availability and as a link between translation regulation and metabolism (Laxman et al., 2013).

In yeast, 5-methoxycarbonylmethyl-thio-uridines (mcm^5s^2Us) found at the wobble position of $tRNA_K^{UUU}$, $tRNA_Q^{UUG}$, and $tRNA_E^{UUC}$ represent an "Achilles heel" exploited by fungal species producing so-called killer toxins. The *Kluyveromyces lactis* killer toxin (also named zymocin) contains a tRNA endonuclease, the γ-toxin, that specifically cleaves these modified tRNAs, resulting in cell-cycle arrest (Lu et al., 2005). As yeast strains lacking the modified tRNAs become resistant to the toxin, several independent mutational screens based on this phenotype have identified genes that are involved in the underlying modification cascade (Butler et al., 1994; Frohloff et al., 2001; Huang et al., 2008; Kishida et al., 1996). Complementation analysis of the *kti* class of mutants identified the six core subunits of the highly conserved eukaryotic Elongator complex (Elp1/Kti7, Elp2/Kti3, Elp3/Kti8, Elp4/Kti9, Elp5, and Elp6/Kti4) and four additional factors, Kti11, Kti12, Kti13, and Kti14, all of which are involved in tRNA modification (Bär et al., 2008; Frohloff et al., 2001; Mehlgarten and Schaffrath, 2003; Zabel et al., 2008).

The eukaryotic Elongator complex was originally described as a transcription elongation factor (Otero et al., 1999), but later was also shown to be required for formation of 5-carbamoylmethyl-uridine and 5-methoxycarbonylmethyl-uridine (mcm^5U) (Huang et al., 2005). HoloElongator contains two copies of each of its six subunits (Glatt et al., 2012a), and each of the subunits is required for the modification reaction. Although the genuine role of Elongator is still under debate (Glatt et al., 2012b) and the details of the tRNA modification reaction carried out by the catalytic Elp3 subunit are not fully understood yet (Chen et al., 2011; Selvadurai et al., 2014), structural and functional analyses of the different Elongator subunits provided support for a direct role of Elongator in wobble uridine modification (Di Santo et al., 2014; Glatt et al., 2012a). Kti11, Kti12, Kti13, and Kti14 appear to fulfill regulatory functions and are only transiently associated with Elongator. The roles of these regulatory factors and at which step of the modification reaction they are required are still unclear.

Kti11, also known as Dph3, is not only involved in Elongator function but also in the biosynthesis of diphthamide, a posttranslational modification of the eukaryotic translation elongation factor 2 (eEF2) (Liu and Leppla, 2003). The formation of this unique

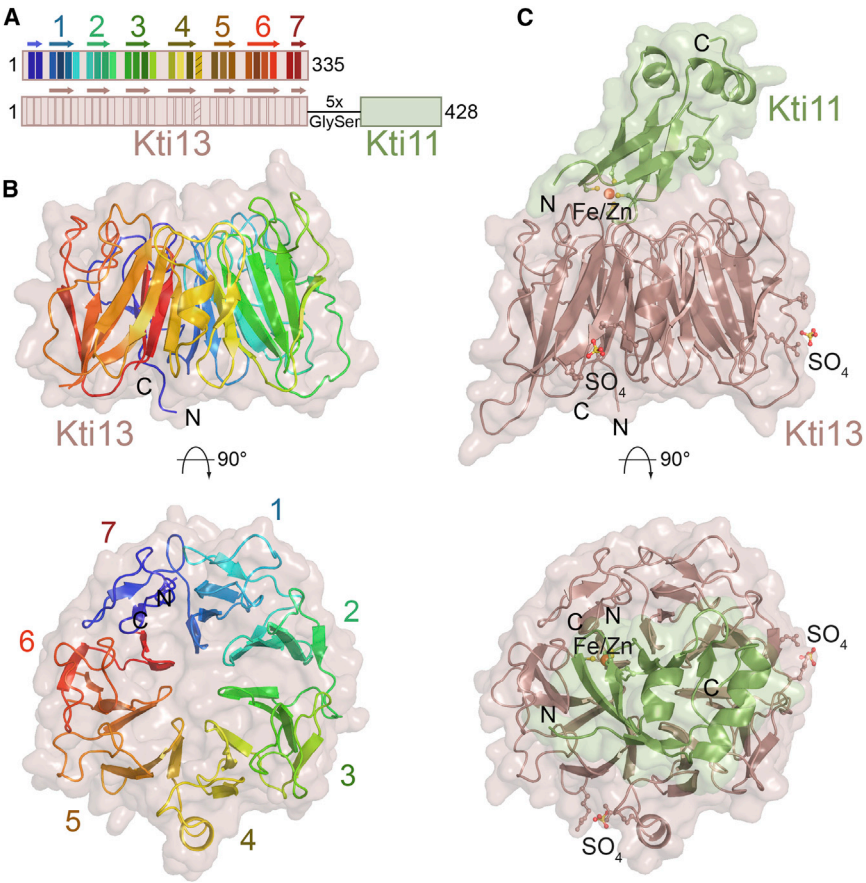

Figure 1. Crystal Structures of Kti13 and the Kti11/Kti13 Heterodimer

(A) Schematic overview of secondary structure elements in the seven-bladed β-propeller protein Kti13 and the Kti13-$(GS)_5$-Kti11 fusion protein.

(B) Crystal structure of Kti13 shown in cartoon and surface representation in two orthogonal views. β sheets are numbered and colored as in (A) and N termini and C termini are labeled.

(C) Crystal structure of Kti11 (green) in complex with Kti13 (dark salmon) shown in cartoon and surface representation in two orthogonal views. Orientation of Kti13 is identical as in (B), and metal binding cysteines (yellow), bound iron or zinc (orange), and bound sulfates (red) are shown in ball-and-stick representation.

See also Figures S1–S3.

histidine modification involves seven so-called diphthamide biosynthesis proteins (Dph1–Dph7) (Abdel-Fattah et al., 2013) and depends on the formation of iron-sulfur clusters in Dph1 and Dph2 (Dong et al., 2014). Although eEF2 is essential for translation (Jørgensen et al., 2006), the genuine role of the diphthamide modification is not fully understood yet. The modified histidine in eEF2 itself, similar to mcm^5s^2U-modified tRNAs, represents a target site for toxins, namely, the ADP-ribosylating diphtheria toxin (Pappenheimer, 1977), the *Pseudonomas aeruginosa* exotoxin A (Zhang et al., 2008), and cholix toxin from *Vibrio cholera* (Jørgensen et al., 2008).

The atomic structure of the small and highly conserved Kti11 protein has been solved by nuclear magnetic resonance (NMR). It uses two zinc knuckles to coordinate a single zinc ion by four cysteine residues, which categorized it into a group of zinc binding proteins with a zinc ribbon fold (Proudfoot et al., 2008; Sun et al., 2005). Kti13, also known as Ats1 (α-tubulin suppressor 1), was originally identified as a suppressor of class 2 α-tubulin mutations (Kirkpatrick and Solomon, 1994). However, as for Kti11, the genuine function of Kti13 in the cell remains elusive. Kti11 and Kti13 interact with each other and stay associated with each other even in the absence of properly assembled Elongator (Zabel et al., 2008). In contrast, the molecular details of Kti11/Kti13 heterodimer formation as well as the molecular function of the Kti11/Kti13 heterodimer are poorly understood. Interestingly, the human Kti13-related protein DelGEF (deafness locus related putative guanine nucleotide exchange factor) and DelGIP, a Kti11 homolog, are both implicated in the development of hereditary deafness in human (Uhlmann et al., 1999). Human DelGIP and DelGEF share 45% and 29% identical amino acid residues with *Saccharomyces cerevisiae* Kti11 and Kti13, respectively, and both proteins also form a heterodimer (Sjölinder et al., 2004). Here, we present the crystal structures of *S. cerevisiae* Kti13 in complex with Kti11 and Kti13 in its unbound form. We validate our crystallographic studies by NMR chemical shift analysis of the heterodimeric Kti11/Kti13 complex in solution and analyze the contribution of individual residues to the interaction surface by mutational studies. We show that Kti11 is binding iron in living yeast cells and provide evidence that heterodimerization itself, and the direct binding of metals to the Kti11/Kti13 heterodimer, influences downstream activation of diphthamide biosynthesis and Elongator-mediated tRNA modification.

RESULTS

Kti13 Is a WD40 Protein

We expressed full-length *S. cerevisiae* Kti13 protein in *Escherichia coli*, purified it using affinity and size exclusion chromatography (Figure 1A and Figure S1A available online), and subsequently carried out crystallization trials. Crystals were obtained after 2 days by the vapor diffusion method and continued growing to sizes suitable for diffraction data collection until day 7. We were able to collect diffraction data up to 2.4 Å resolution. The crystal structure of Kti13 was determined using selenomethionine-substituted protein in a single anomalous dispersion experiment and subsequently refined to R_{work}/R_{free} values of 23.5%/26.1% (Table 1). Kti13 shows a typical WD40 domain fold with seven antiparallel β stranded blades. In detail, blades 1, 2, 3, 6, and 7 are built up by four β strands, whereas blades 4 and 5 contain only three β strands. The three β strands of blade 4 and 5 are complemented by the presence of a short helix and an extended loop, respectively. Blade 7 is stabilized by β strand

Table 1. Data Collection and Refinement Statistics

	Kti13 SeMet	Kti11/Kti13 $P6_4$	Kti11/Kti13 $P6_4$ (Fe Edge)	Kti11/Kti13 $P6_5$
Data Collection				
Beamline	ID14-4 (ESRF)	P14 (PETRAIII)	P14 (PETRAIII)	P14 (PETRAIII)
Space group	$P2_1$	$P6_4$	$P6_4$	$P6_5$
Cell dimensions				
a, *b*, *c* (Å)	35.75, 96.6, 97.35	151.27, 151.27, 107.14	152.46, 152.46, 107.46	152.06, 152.06, 203.85
α, β, γ (°)	90, 95.62, 90	90, 90, 120	90, 90, 120	90, 90, 120
Wavelength (Å)	0.97914	0.97626	1.69696	0.97626
Resolution (Å)[a,b]	50–2.4 (2.46–2.4)	50–2.9 (2.97–2.9)	50–3.5 (3.58–3.5)	50–3.0 (3.08–3.0)
CC(1/2)	0.99 (0.49)	0.99 (0.55)	0.99 (0.68)	0.99 (0.47)
R_{merge} (%)	10.3 (268.6)	9.8 (155.3)	13.9 (107.7)	11.3 (195.3)
I/σI	11.88 (0.75)	20.33 (1.5)	16.17 (1.79)	17.05 (1.23)
Completeness (%)	99.8 (98.1)	99.4 (94.1)	99.5 (93.2)	99.6 (94.9)
Redundancy	9.3 (8.9)	11.0 (10.0)	10.0 (6.9)	11.4 (11.1)
Sites	12 Se		2 Fe	
Refinement				
Resolution (Å)	50–2.4	50–2.9		50–3.0
No. of reflections	25,852	30,906		53,186
R_{work}/R_{free} (%)	23.55/26.06	19.99/21.9		20.86/23.47
No. of atoms				
Protein	4,970	6,329		12,686
Ligand	0	17		29
Water	0	0		0
B-factors (Å^2)				
Protein	61.08	50.5		95.35
Ligand		95.0		134.7
rmsd				
Bond lengths (Å)	0.002	0.003		0.002
Bond angles (°)	0.492	0.605		0.509

[a]Values in parentheses correspond to the highest resolution shell.
[b]Resolution cutoff criteria according to (Karplus and Diederichs, 2012). Resolution limits according to an I/σ(I) of 2 are 2.6 Å for Kti13, 2.95 Å for Kti11/Kti13 in $P6_4$, and 3.1 Å for Kti11/Kti13 in $P6_5$.

completion, where the most C-terminal strand (residues 330–334) and the most N-terminal strand (residues 5–10) form a "Velcro-like" closure completing the last blade (Figure 1B). Structural comparisons revealed that among the WD40 protein family, Kti13 showed highest similarity to regulator of chromosome condensation 1 (RCC1) and other RCC1-like domains. The central cavity of the WD40 domain is wide, and the individual strands of the propeller are connected by large loops that nevertheless can be nicely traced in the density. Using gel filtration and analytical ultracentrifugation analyses, we show that Kti13 is present as a monomer in solution (Figures S1A and S1B). Surface conservation analyses revealed a highly conserved surface patch at the top side of the propeller, which is known from other WD40 proteins as a "super-site" for protein-protein interactions (Stirnimann et al., 2010). This region in Kti13 contains several solvent-exposed hydrophobic residues, which also indicates a suitable interaction site for binding a protein partner (Figures S1C and S1D).

WD40 domain proteins, such as Kti13, are not only well-known protein binding domains but also some of them are known to specifically interact with lipids. We therefore tested purified Kti13 in a physiological and quantitative lipid binding assay that is based on the use of artificial, surrogate membranes (liposomes) and allows protein-lipid interactions to be studied in the context of a membrane bilayer (Table S3) (Saliba et al., 2014). Strikingly, GFP-tagged Kti13 was efficiently and specifically recruited to liposomes containing either phosphatidylinositol 3,4-bisphosphate [PI(3,4)P_2] or phosphatidylinositol 4,5-bisphosphate [PI(4,5)P_2] in this assay that approximates the in vivo situation (Figures S2A and S2B). Its binding specificity was similar to that of the pleckstrin homology domain of Plcδ, known to recognize PI(4,5)P_2 (Figures S2A and S2C).

Structure of the Kti11/Kti13 Heterodimer

Kti13 interacts with Kti11 in vivo (Zabel et al., 2008), and here we show that both purified proteins also interact in vitro with high affinity (see below). Because initial crystallization trials of the reconstituted heterodimeric complex did not yield crystals, we expressed a fusion protein [Kti13-$(GS)_5$-Kti11], in which the two proteins were connected using a ten-amino-acid (5× Gly-Ser)

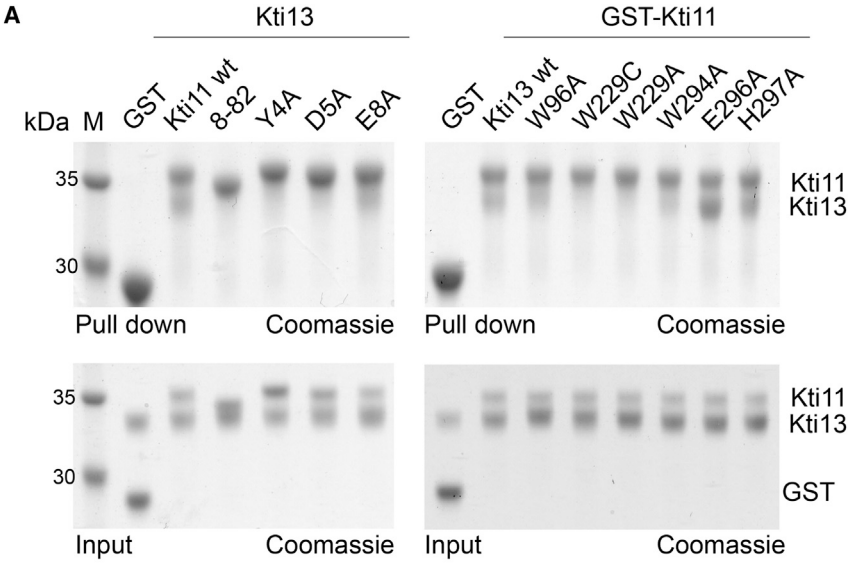

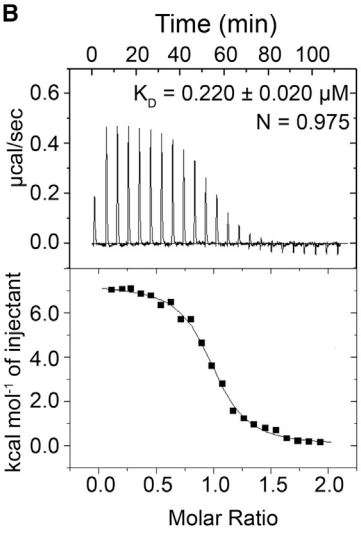

C

Cell	Syringe	K_D (µM)
Kti13 wt	Kti11 wt	0.220 ± 0.020
Kti13 W96A	Kti11 wt	0.585 ± 0.050
Kti13 W229A	Kti11 wt	4.630 ± 0.772
Kti13 W294A	Kti11 wt	0.295 ± 0.020
Kti13 E296A	Kti11 wt	0.012 ± 0.001
Kti13 H297A	Kti11 wt	0.083 ± 0.006
Kti13 wt	Kti11 Y4A	> 100
Kti13 wt	Kti11 D5A	> 100
Kti13 wt	Kti11 Y4AD5A	> 100
Kti13 wt	Kti11 E6A	0.917 ± 0.172
Kti13 wt	Kti11 E8A	3.021 ± 1.314
Kti13 wt	Kti11 E6AE8A	5.128 ± 1.060

Figure 2. Mutants of the Kti11/Kti13 Dimer Interface

(A) Left: GST-pull-down assays of purified GST-tagged Kti11 variants with untagged Kti13. A mixture of purified GST and untagged Kti13 was used as control. Lower gel shows 5% of the input and upper gel shows bound fractions. Right: GST-pull-down assays of purified untagged Kti13 variants with GST-tagged Kti11. Lower gel shows 5% of the input and upper gel shows bound fractions.

(B) ITC measurement using purified Kti13 (10 µM in the cell) and Kti11 (100 µM in the syringe). Calculated K_D values and stoichiometry (N) are indicated.

(C) Summary of ITC measurement using indicated Kti11 and Kti13 single point mutants.

See also Figure S4.

linker (Figure 1A). This strategy has been successfully applied to a variety of protein complexes in crystallography and electron microscopy in order to ensure precise 1:1 stoichiometry or to stabilize protein complexes (Reddy Chichili et al., 2013). We obtained crystals in two different space groups ($P6_4$ and $P6_5$) that allowed collecting diffraction data up to 2.9 and 3.0 Å resolution, respectively. The complex structures could be solved by molecular replacement using the Kti13 structure as a search model and subsequently refined to R_{work}/R_{free} values of 20.0%/21.9% and 20.9%/23.5% (Table 1). In the complex structure, Kti11 indeed binds to Kti13 through the conserved hydrophobic region on top of the WD40 propeller (Figure 1C). Comparison of the unbound Kti13 structure with the Kti11-bound form of Kti13 shows that there are no overall structural rearrangements in Kti13 upon complex formation (root-mean-square deviation $[rmsd]_{326C\alpha}$ = 0.78 Å). Somehow unexpected, in the crystals Kti11 binds to a neighboring Kti13 molecule, but not the covalently linked Kti13 molecule of the fusion construct (Figure S3). Although the linker regions themselves are in different conformations, the six different Kti11/Kti13 complexes present in the asymmetric units of the two crystal forms show an almost identical arrangement of the two proteins (Figure S3). We therefore conclude that the observed Kti11/Kti13 heterodimer is reflecting the native relative orientation.

Validation of the Kti11/Kti13 Heterodimer Interface

We further assessed the Kti11/Kti13 interface by using structure-guided single point mutations in different biochemical interaction assays using individually purified Kti11 and Kti13 proteins. We observed a strong decrease in affinity toward Kti13 using N-terminally truncated Kti11 (8–82), Kti11-Y4A, or Kti11-D5A in glutathione S-transferase (GST)-pull-down assays, whereas the Kti11-E8A mutation had a less severe effect on the interaction (Figure 2A, left). These results clearly confirmed the involvement of conserved residues in the N terminus of Kti11 in the interface with Kti13, as seen in our crystal structures. In addition, we tested several highly conserved Kti13 residues (Figure 2A, right) that, based on the structures, are thought to contribute to the interaction surface (Figure S4A). Mutating the most central hydrophobic tryptophan residue of Kti13 (W229A/C) in the interface almost abolished binding, while the variant Kti13-W96A only showed reduced affinity to Kti11. The side-chain orientation of residue W294 of Kti13 is considerably different in the binding interface of Kti11/Kti13 compared to unbound Kti13. Accordingly, replacing W294 with alanine slightly reduced the affinity of Kti13 toward Kti11 (Figure 2A). Mutating other residues in the proximity of the interaction site (Kti13-E296A and Kti13-H297A) had no detectable negative effect on binding, or even enhanced the interaction (Figure 2A). As E296 and H297A are in close proximity to W294 (Figure S4A), we speculate that mutating these residues to alanine enhances the degree of freedom for the W294 side chain, allowing it more easily to adapt the conformation observed in the complex structure

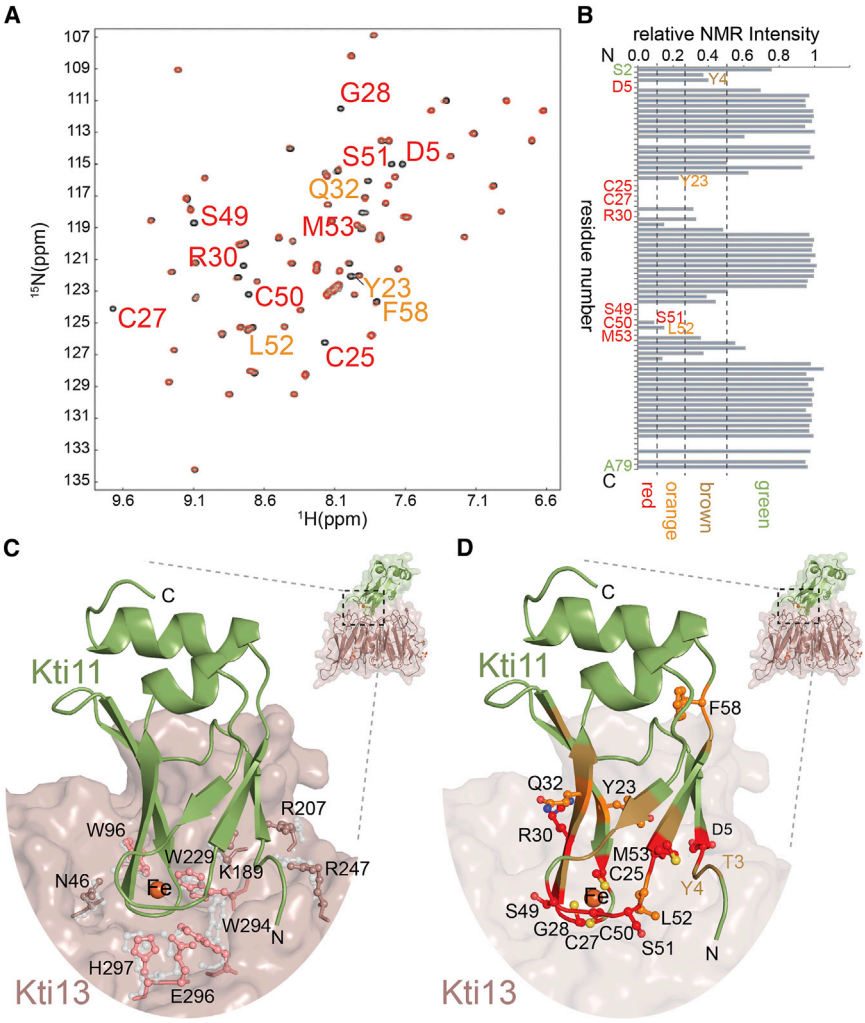

Figure 3. NMR Analysis of the Kti11/Kti13 Heterodimer

(A) ^{1}H-^{15}N HSQC spectra of N^{15}-labeled Kti11 in the absence (black) and presence of 15 μM Kti13 (red). Residue numbers are indicated for peaks that show strong (red) and clear (orange) differences.

(B) Quantified NMR intensities blotted for all Kti11 residues. Selected residues are highlighted and colored according to (A).

(C) Close-up view of Kti11 bound to Kti13 with interacting residues of Kti13 residues labeled and displayed in ball-and-stick representation. Conformations of the residues in the unbound Kti13 structure are colored gray.

(D) Close-up view of Kti11 (green, cartoon) bound to Kti13 (dark salmon, surface) with residues labeled and colored as indicated in (A) and (B).

See also Figure S5.

and thereby increasing the affinity of these mutants for Kti11. We could not detect severe changes in the integrity or stability of Kti11 and Kti13 as judged by size exclusion chromatography and thermostability analyses (Figures S4B and S4C), consistent with the view that the Kti11 and Kti13 mutations only affect the interaction with each other, but not the integrity of Kti11 and Kti13 themselves.

To analyze the binding affinity between Kti11 and Kti13 more quantitatively, we also used isothermal titration calorimetry (ITC) and analytical ultracentrifugation. Using ITC, we found that the untagged Kti11 (Figure S5A) and Kti13 (Figure S1A) proteins bind each other with high affinity (K_D = 220 nM) in a 1:1 stoichiometry (Figure 2B), which agrees with results from analytical ultracentrifugation where Kti11 and Kti13 also form a 1:1 complex (Figure S5B). Subsequently, we analyzed the consequences of the above-described mutants on heterodimer formation using ITC. Thereby, we confirmed the results from the GST pull-down assays, i.e., that residues in the N terminus of Kti11 (Y4 and D5) and the most central tryptophan residue (W229) of Kti13 are most critical for heterodimer formation. Mutant proteins Kti11-Y4A and Kti11-D5A show more than 450-fold lower affinity, while for mutant protein Kti13-W229A, the affinity is decreased by a factor of 21 (Figure 2C). More peripheral residues (e.g., E6, E8, W96, and W294) contribute less to the complex affinity, and substituting E296 or H297 in Kti13 even increased the affinity of Kti11 to Kti13 (Figure 2C).

To further validate the interaction of Kti11 and Kti13 in solution, we used NMR spectroscopy. ^{15}N-labeled Kti11 was prepared in the presence of iron, and the cross-peaks in the 2D ^{1}H-^{15}N heteronuclear single quantum coherence (HSQC) spectrum (Figure 3A) were assigned according to the NMR structure of zinc-bound Kti11 (Sun et al., 2005, Figure S5C). Subsequent titration with non-labeled Kti13 caused changes of the NMR resonances of a number of Kti11 residues (Figures 3A and 3B). In addition to several Kti11 residues close to the iron binding site (C25, C27, G28, R30, S49, C50, S51, and M53), highly conserved Kti11 residues of the N terminus, namely, Y4 and D5, were affected by the interaction with Kti13. In conclusion, all residues showing significant changes in affinity or NMR resonances upon complex formation are in close proximity to the interaction surface observed in the crystal structure of the complex, thereby confirming that Kti11 interacts with Kti13 in solution as observed in the crystal structure (Figures 3C and 3D).

Kti11/Kti13 Heterodimer Formation Is Required for Modifications of tRNAs and eEF2

As Kti11 and Kti13 are both essential for the proper modification of tRNAs by Elongator, and Kti11 is a known component of the diphthamide modification pathway, we were curious whether the direct interaction of these two proteins is required for the activation of these two translational control mechanisms. First, we could confirm that residues in the N terminus of Kti11 and Kti13-W229 are also essential for proper complex formation in vivo by coimmunoprecipitation assays (Figures 4A and 4B). Yeast strains lacking Elongator-dependent mcm^{5}s^{2}U

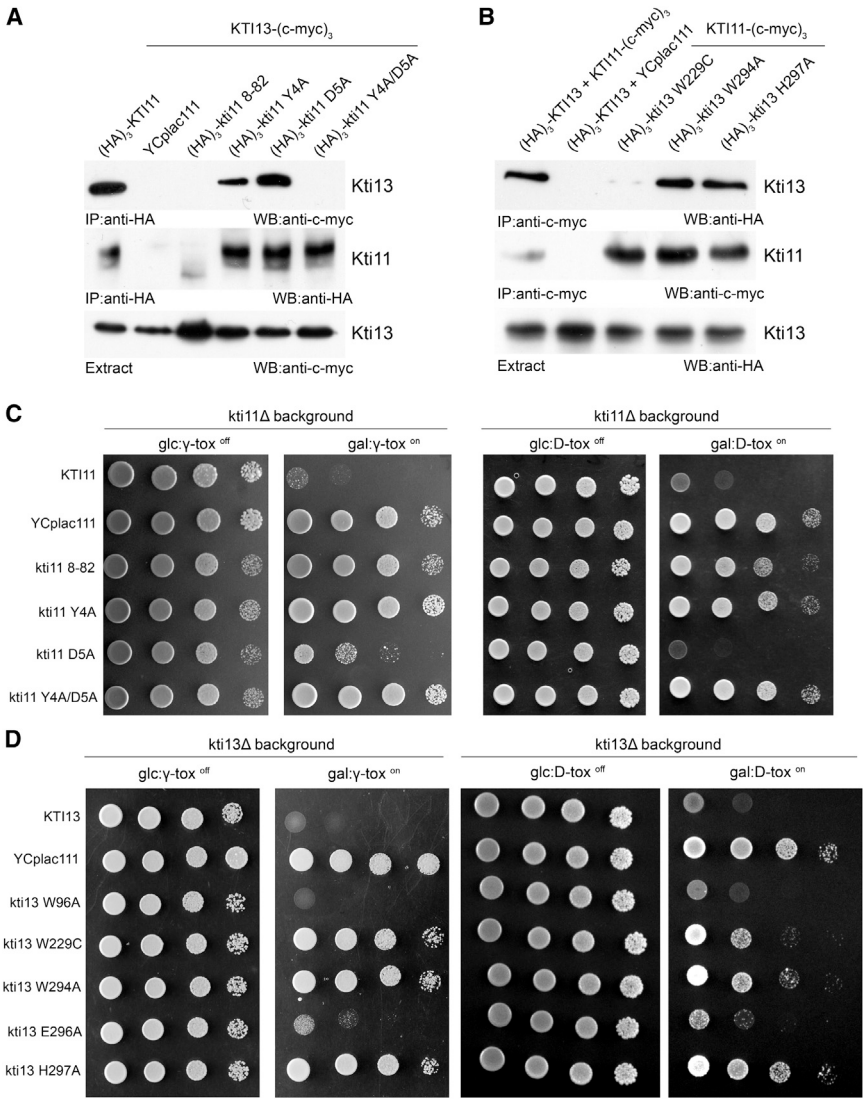

Figure 4. Phenotypical Characterization of Dimer Interface Mutants

(A) The indicated yeast strains expressing HA-tagged variants of Kti11 and myc-tagged Kti13 were subjected to immunoprecipitations (IP) using anti-HA antibody. The upper blot was probed with an anti-c-*myc* antibody to detect coimmunoprecipitated Kti13 protein levels. The middle blot was probed with an anti-HA antibody to control for precipitation of HA-tagged Kti11 protein. The lower blot was probed with anti-c-*myc* antibody to detect input levels of Kti13 protein in the used extracts. The combination of myc-tagged Kti13 with an empty vector (YCplac111) served as background control.

(B) Same as (A) with HA-tagged variants of Kti13 and myc-tagged Kti11. The combination of wild-type HA-tagged Kti13 with an empty vector [$(HA)_3$-KTI13 + YCplac111] served as background control.

(C) Phenotypes of the respective Kti11 mutant strains from (A) tested in the γ-toxin and D-toxin assays in a *kti11* deletion background.

(D) Phenotypes of the respective *kti13* mutant strains from (B) tested in the γ-toxin and D-toxin assays in a *kti13* deletion background.

See also Figure S6.

modifications in tRNA anticodons or the eEF2-diphthamide modification synthesized by the DPH complex develop resistances against γ-toxin or diphtheria toxin and grow under conditions where strains carrying these modifications cannot survive. Therefore, we used established toxin assays (Frohloff et al., 2001; Mattheakis et al., 1992) to ask whether the above-described mutants affect the activity of the downstream modification pathways (Figures 4C, 4D and S6). Consistent with the interaction data (Figure 4A), the deletion of the N-terminal seven amino acids (*kti11-8_82*) as well as the *kti11-Y4A* allele conferred γ-toxin and diphtheria toxin resistance. Likewise, the *kti13-W229C* mutant was resistant and impaired in Kti11 interaction. Although Kti11-D5A showed a strong reduction of affinity in our in vitro interaction assays, we could not detect any reduction in vivo, also explaining its weak toxin phenotype. The reason for this apparent discrepancy is unclear to us. Nevertheless, D5 seems to contribute to the interaction with Kti13 also in vivo, as the combination of Y4A and D5A (Y4A/D5A) further decreased the affinity of the Y4A mutant toward Kti13 in vivo. None of the described amino acid substitutions appear to affect the integrity of the proteins. Hence, we conclude that the ability to form the Kti11/Kti13 dimer directly affects the activity of Elongator and the DPH complex.

Whereas heterodimer formation is necessary to support both modification reactions, it does not seem to be sufficient. Interestingly, the Kti13-H297A mutant, which shows higher affinity toward Kti11 in vitro, conferred γ-toxin and diphtheria toxin resistance. Similarly, the *kti13-W294* mutant was toxin resistant but Kti11 binding proficient in vivo (although it showed slightly reduced affinity for Kti11 in vitro; Figure 2C). There is also evidence that Elongator-dependent tRNA modification and diphthamide biosynthesis functions can be separated by mutations. The Kti11-E6A/E8A variant gave γ-toxin resistance and diphtheria toxin sensitivity (Figure S6C), indicating that some residues in the N terminus of Kti11 are important for Elongator activity, but not for DPH activity. In summary, we have used our structural and biochemical insights to identify several single point mutations in Kti11 and Kti13 that lead to reduced levels of mcm^5s^2U-modified tRNAs and diphthamide in living yeast cells.

Zinc- and Iron-Bound Forms of Kti11 Are Able to Interact with Kti13

We further tried to understand the prerequisites of metal ion coordination in Kti11 and its consequences for Kti11/Kti13 heterodimerization and downstream signaling. First, we compared the two independently determined NMR structures of Kti11 bound to zinc (Protein Data Bank [PDB] ID codes 1YWS and 1YOP) with the crystal structure of Kti11 in complex with Kti13. There are

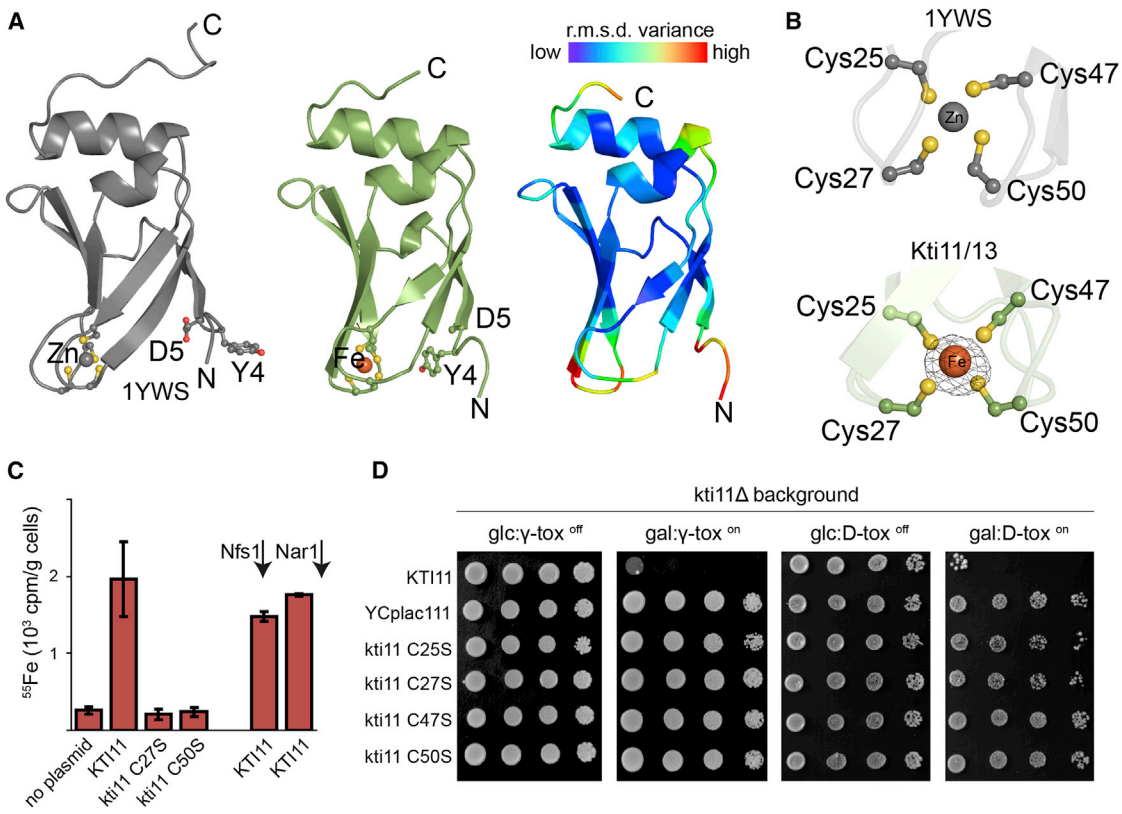

Figure 5. Metal Binding Is Essential for Kti11 Function

(A) Structural comparison of zinc-bound Kti11 (gray, PDB ID code 1YWS) and Kti13-bound Kti11 (green), both shown in cartoon representation. Metal binding residues and conserved residues in the N terminus are labeled and shown in ball-and-stick representations. Heatmap of structural variance is shown on the right.

(B) Close-up of the metal binding sites in zinc-bound Kti11 (top representation) and Kti13-bound Kti11 (bottom representation). Anomalous difference Fourier map (λ = 1.6969 Å) is shown at 5 σ for the Kti13-bound Kti11.

(C) Incorporation of radioactively labeled iron (^{55}Fe) into Kti11 was tested in wild-type yeast (W303; left), Gal-NFS1 yeast strains, and Gal-NAR1 yeast strains. Kti11 protein carrying mutations in the metal binding site (C27S and C50S) does not show any residual iron incorporation. Depletions of iron-sulfur protein biogenesis factors (Nfs1 and Nar1) by growth of the Gal strains on glucose-containing medium do not affect ^{55}Fe incorporation into Kti11 in vivo. Error bars represent SDs of the replicates (n = 4 except for Nar1 and no plasmid where n = 2).

(D) Influence of mutations in the metal binding site (C25S, C27S, C47S, and C50S) on γ-toxin and diphtheria toxin sensitivity. *KTI11* alleles were introduced on a YCplac111 based centromeric plasmid in a W303-derived *kti11* deletion strain.

See also Figure S7.

no obvious structural rearrangements in Kti11 upon Kti13 binding. The overall rmsd between the Kti11 X-ray and the two known NMR structures is lower ($rmsd_{71C\alpha}$ = 1.51 Å [1YWS]/$rmsd_{71C\alpha}$ = 1.81 Å [1YOP]) than the difference between the two NMR structures themselves ($rmsd_{71C\alpha}$ = 2.19 Å). Slight structural differences are observed in the region of the zinc binding motif and in the N-terminal residues 1–5 involved in heterodimerization with Kti13 (Figure 5A). Purified Kti11, the Kti11/Kti13 complex, and the crystals of Kti13-$(GS)_5$-Kti11 showed a reddish color, an indicator for the presence of iron. We used X-ray fluorescence spectroscopy to analyze the chemical content of the Kti11/Kti13 crystals. We could observe X-ray fluorescence emission peaks at similar height for zinc and iron in the crystals (Figure S7A), suggesting that zinc and iron are present in comparable amounts in Kti11. To locate the iron binding site in the protein, we collected a full data set close to the absorption edge of iron (λ = 1.6969 Å). At this wavelength the f″/f′ values for iron and zinc are 3.73/−2.74 e and 0.84/−1.22 e, respectively, demonstrating that zinc contributes little to the anomalous signal. After calculating an anomalous difference Fourier map, using phases from the refined model, we could detect clear anomalous difference peaks in the center of the proposed "zinc knuckles," confirming that iron binds in the same site as zinc (Figure 5B). A characteristic rubredoxin-like UV-visible absorption spectrum was observed with our purified Kti11 preparations and was absent in purified Kti11 variants lacking one of the cysteine residues (Figure S7B). In conclusion, we show that the previously identified zinc binding site is identical with the iron binding site, that coordination of different metals does not influence Kti11/Kti13 heterodimerization, and vice versa that Kti11/Kti13 heterodimerization does not influence the metal specificity of Kti11 in vitro.

Kti11 Is Able to Bind Iron in Yeast Cells

We further addressed the question of whether Kti11 is able to bind iron not only in vitro but also in vivo. Therefore, we incubated yeast strains transformed with a plasmid encoding a

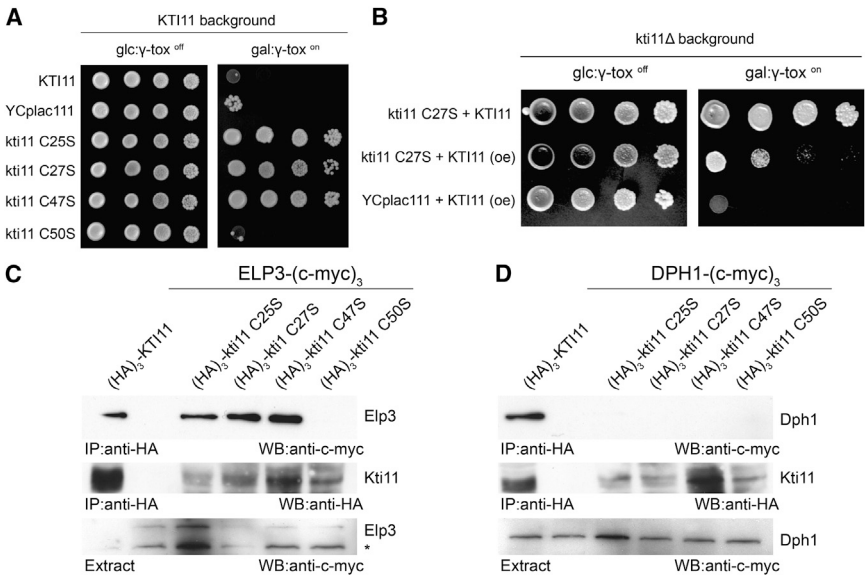

Figure 6. Metal Binding Is Important for Kti11 Downstream Signaling

(A) Same as in Figure 5D, but plasmids were introduced into a *KTI11* wild-type strain.

(B) Influence of *KTI11* overexpression (oe) on γ-toxin sensitivity. Multicopy YEplac195-based *KTI11* plasmid was introduced into the *kti11* mutant strain carrying centromeric *kti11-C27S* plasmid or empty vector (YCplac111) control.

(C) Coimmunoprecipitation of Elp3-(c-*myc*)$_3$ (upper blot) with (HA)$_3$-Kti11 (middle blot). Yeast strain containing a c-*myc*-tagged *ELP3* allele was transformed with plasmids carrying *(HA)$_3$-KTI11* alleles. Cell lysates were immunoprecipitated with α-HA antibodies and pellet fractions (IP) or total lysates (Extract; lower blot) were analyzed by western blotting (WB).

(D) Same as in (C) using Dph1-(c-*myc*)$_3$ with *(HA)$_3$-KTI11* alleles.

See also Figure S8.

hemagglutinin (HA)-tagged version of wild-type Kti11 with radioactive iron (^{55}Fe) and analyzed the incorporation of iron into Kti11 in vivo by measuring the radioactivity of Kti11 by immunoprecipitation via its affinity tag. Nontransformed wild-type yeast cells, and two strains expressing tagged versions of Kti11 carrying point mutations in cysteine residues C27S and C50S responsible for the metal binding in vitro (Figure 5B), served as controls. We detected radioactive labeling of wild-type Kti11, whereas only background signals were detected in the precipitates of Kti11 cysteine mutants (Figure 5C). The Kti11 iron levels remained almost unchanged after the depletion of proteins involved in iron-sulfur protein biogenesis, namely, Nfs1 and Nar1 (Figure 5C). Therefore, we conclude that Kti11 is able to incorporate iron in living yeast cells and does not require the iron-sulfur protein biosynthesis machinery for this incorporation.

We subsequently tested mutants lacking any one of the crucial cysteine residues for iron coordination (C25S, C27S, C47S, and C50S) in γ-toxin and diphtheria toxin resistance assays. None of the four mutated versions of Kti11 could rescue the γ-toxin and diphtheria toxin resistance of a *kti11* deletion strain (Figure 5D), indicating that iron coordination by Kti11 is equally important for tRNA modification and diphthamide biosynthesis. We further tested the influence of the four cysteine mutations in a *KTI11* wild-type background by γ-toxin and diphtheria toxin resistance assays. All four mutants were sensitive in the D-toxin assay, indicating that the wild-type allele of *KTI11* is able to compensate for loss of function conferred by the *kti11* alleles (Figure S7C). In contrast, the C25S, C27S, and C47S mutations resembled the *KTI5* allele (Huang et al., 2008), showing a dominant-negative phenotype in the γ-toxin assays, whereas the C50S mutant is recessive (Figure 6A). In agreement with the idea of a concentration-dependent competition for a binding site, we show that the overexpression of wild-type Kti11 is able to partially rescue the dominant-negative phenotype induced by the introduction of C27S into a *kti11* background (Figure 6B). This observation indicates that while the coordinated metal is essential for the function of Kti11 for both modification reactions, a metal-free version of Kti11 is able to functionally compete with the metal-bound form of Kti11 only in the tRNA modification pathway. As the cysteine mutants are still able to interact with Kti13 in vivo (Figure S7D), we tested whether the competition occurs on downstream targets of Kti11. Strikingly, the mutants displaying a dominant-negative phenotype are all able to interact with Elongator in vivo, whereas the recessive C50S mutant shows no detectable interaction with Elongator (Figure 6C). In contrast, all four cysteine mutants do not interact with Dph1 (Figure 6D). In summary, we show that the ability of C25S, C27S, and C47S to block the function of the wild-type protein is specifically related to the tRNA modification pathway.

DISCUSSION

In eukaryotic cells, biosynthesis of mcm^{5}U34-modified tRNAs and diphthamide-modified eEF2 requires the highly conserved protein complexes Elongator and DPH complex, respectively. Here, we show that in yeast these two different modification reactions both require the Kti11/Kti13 heterodimer. According to our structural analysis, neither Kti11 nor Kti13 undergoes major structural rearrangements upon heterodimerization. However, we observed strong functional consequences for the downstream modification reactions if heterodimer formation is impaired.

Based on the crystal structure of the Kti11/Kti13 heterodimer, we were able to generate structure-guided single point mutations at the interface of Kti11 and Kti13 that abolish heterodimer formation without affecting the structural integrity of the individual proteins. The strongest mutant affecting heterodimer formation in Kti13, namely, W229C, is located in the very center of the identified Kti11/Kti13 interface. Notably, the *W229C* mutant (*kti13-5*) was also isolated in the first screen for factors conferring zymocin resistance (Butler et al., 1994). In addition, we identified highly conserved N-terminal residues in Kti11, namely, Y4 and D5, that are equally essential for Kti11/Kti13 heterodimer formation. As probed by γ-toxin and diphtheria toxin for the tRNA and diphthamide biosynthetic reactions, respectively, DPH and Elongator functions both require Kti11/Kti13 interaction.

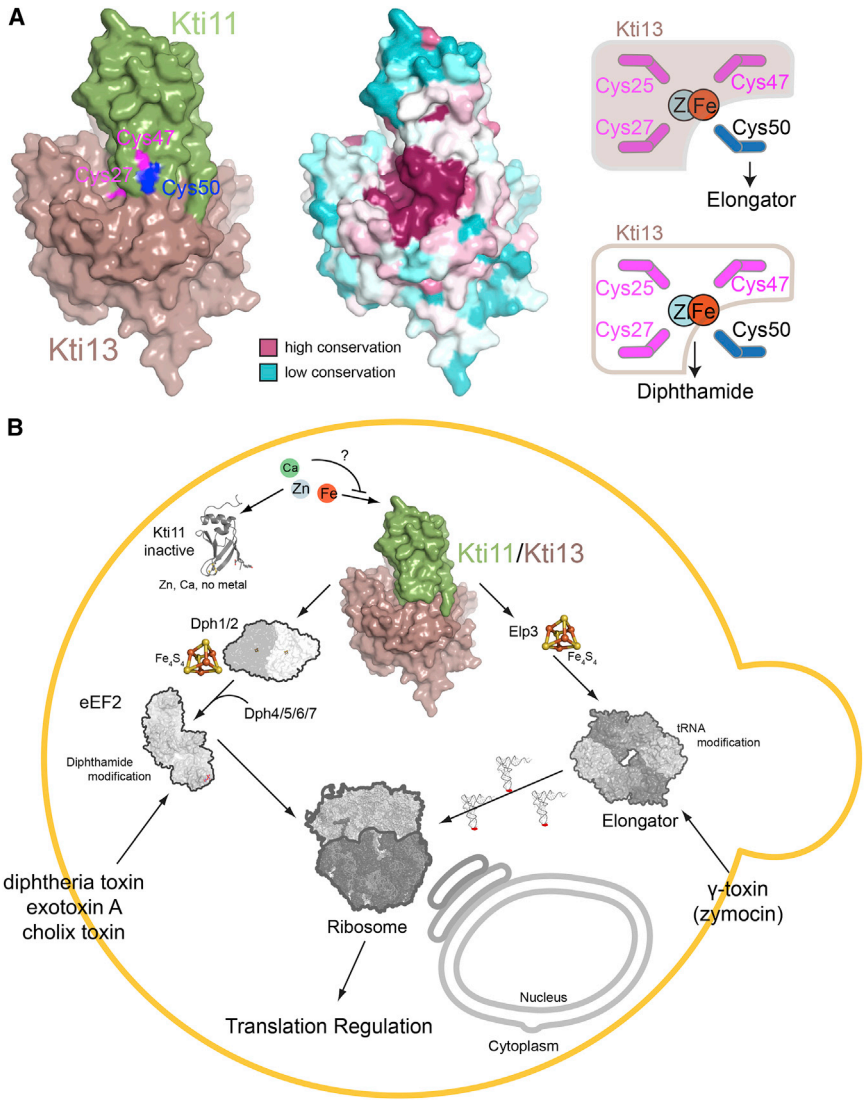

Figure 7. Model of the Differential Activation of Elongator and Diphthamide Biosynthesis by the Kti11/Kti13 Heterodimer

(A) Localization of the metal binding site of Kti11 in the Kti11/Kti13 heterodimer (left). Surface representation of Kti11/Kti13 colored by conservation scores (middle). Current model of how Kti11 and Kti13 communicate with their downstream effectors: only residue C50 directly contacts Elongator, while all metal-coordinating cysteines are required for the interaction with the DPH complex.

(B) Schematic overview of the current working model for Kti11- and Kti13-dependent regulation of Elongator activity, diphthamide biosynthesis, and global translational control.

Interestingly, Kti13-E296A and Kti13-H297A, which both show increased binding affinities to Kti11, exhibit different effects in toxin resistance assays; i.e., H297A is resistant to both toxins, whereas E296A remains sensitive. We therefore conclude that heterodimerization is essential, but not sufficient, for proper downstream activation.

Since Kti13 has never been shown to be directly involved in diphthamide biosynthesis, the possibility remained that the deactivation of the tRNA modification pathway via the deletion or mutation of Kti13 leads to indirect effects on the diphthamide modification pathway. However, the diphtheria toxin resistance phenotype resulting from *kti13* mutations could not be suppressed by overexpressing $tRNA_K^{UUU}$, $tRNA_Q^{UUG}$, and $tRNA_E^{UUC}$ (Figure S8A) known to rescue most of the known Elongator-related phenotypes (Esberg et al., 2006). In addition, a yeast strain where *ELP3*, the gene encoding the enzymatic subunit of the Elongator complex, is deleted remains sensitive to diphtheria toxin (Figure S8B). Our results therefore provide evidence that Kti13 (or the Kti11/Kti13 heterodimer) is directly involved in the regulation of the diphthamide modification pathway.

Interestingly, all the known downstream partners of Kti11, namely, Dph1, Dph2, and Elp3, contain iron-sulfur clusters, which are essential for their respective catalytic reactions (Paraskevopoulou et al., 2006; Zhang et al., 2010). We hypothesize that the Kti11/Kti13 heterodimer provides a function to the iron-sulfur cluster of Elongator and Dph1/Dph2 that requires iron binding to Kti11. During the preparation of this article, Dong et al. (2014) showed that Kti11/Dph3 can indeed act as electron donor for Dph1 and Dph2 in vitro. Our observation that Kti11 is able to complex iron not only in vitro but also in yeast cells further clarifies the functional link between Kti11 and the two chemically distinct modification reactions. Mutation of any of the four conserved cysteines in Kti11 resulted in the inability to bind metal and gives resistance against the microbial γ-toxin and diphtheria toxin. These observations indicate that in addition to Kti11/Kti13 heterodimer formation (see above), metal binding by Kti11 is essential to support both Elongator-dependent tRNA modifications and the diphthamide biosynthesis reaction.

Although the metal binding site is in close proximity to residues in Kti11 and Kti13, which are important for the heterodimerization, metal ion coordination is not required for the Kti13 interaction (Figure S7D). Strikingly, three of the four cysteine mutants (*KTI11-C25S*, *KTI11-C27S*, and *KTI11-C47S*) display a dominant-negative phenotype in tRNA modification; i.e., they interfere with Elongator function in the presence of a wild-type *KTI11* gene. Since these mutant proteins, but not the variant encoded by the recessive *kti11-C50S* allele, are still able to interact with Elongator, we conclude that metal binding is also not required for the Kti11-Elongator interaction and that mutant variants of Kti11 compete with wild-type Kti11 for Elongator binding. Consistently, we were able to partially suppress the dominant-negative phenotype of *KTI11-C27S* by overexpressing wild-type *KTI11.* Residue C50 in Kti11 is the only cysteine that is not masked by Kti13 in the Kti11/Kti13 heterodimer (Figure 7A). Since its replacement by serine abolished the interaction with Elp3 in vivo, we propose that C50

is directly contacting Elongator, while the other three cysteine residues are presumably buried in the interface of the Kti11/Kti13 heterodimer. Interestingly, Kti13-W294 and Kti13-H297, which are not essential for heterodimer formation, but show clear Elongator phenotypes, are in close proximity to Kti11-C50. These findings suggest that this highly conserved surface region of the heterodimer (Figure 7A) carries out important functions required for the downstream activation of Elongator. As metal ion coordination is not required for heterodimer formation (Figure S7D), we propose that Kti11 and Kti13 likely stay associated during metal incorporation and their interaction with Elongator.

In contrast, all four cysteine mutants of KTI11 lose the ability to bind to Dph1 and are recessive in the D-toxin assay, indicating that different from Elongator binding, interaction of the Kti11/Kti13 heterodimer with the Dph1/Dph2 complex requires metal coordination. This suggests that Kti11/Kti13 uses different interfaces to bind to the DPH and Elongator complexes. As metal-free Kti11 is inactive but shows different interaction preferences for the two downstream pathways, our results shed light on the subtle differences in Kti11/Kti13-dependent regulation of its downstream pathways. We hypothesize that Kti11 could also act as a redox sensor or distinguishes different levels of metal ions in the cell to direct downstream reactions once the intracellular metal ion balance is altered (Figure 7B).

Kti13 specifically binds to PI(3,4)P_2 and PI(4,5)P_2 that are enriched in certain cellular compartments, such as the cytosolic side of the cell membrane (Di Paolo and De Camilli, 2006). This observation suggests that Kti13 might be recruited to cell membranes and that its cellular localization contributes to the regulation of the two downstream modification pathways. In support of a more auxiliary role of Kti13 (such as spatial activation), the deletion of Kti13 does not lead to a complete loss rather to a decrease of Elongator's tRNA modification activity (Huang et al., 2008). In addition, it was recently reported that Elp3 from *Toxoplasma gondii* contains a C-terminal transmembrane domain that anchors this protein at the mitochondrial outer membrane (Stilger and Sullivan, 2013).

The Kti11/Kti13 heterodimer is involved in two consecutive steps during the translation process: wobble uridine modification in tRNA has been shown to affect tRNA binding to the A-site on the ribosome, whereas the diphthamide modification alters eEF2 function, thereby affecting the translocation of the peptidyl-tRNA from the A-site to the P-site. The molecular details of the Kti11/Kti13 heterodimer reported here provide insight how Kti11/Kti13 might fulfill its function and whether the properties of Kti11 and Kti13 allow linking tRNA and eEF2 modifications to metabolic signaling pathways.

EXPERIMENTAL PROCEDURES

Cloning, Expression, and Purification

The *S. cerevisiae* Kti13 and Kti11 codon sequences were cloned into pETM30 vector to obtain N-terminally 6×His-GST-tagged proteins, and the resulting plasmids were transformed into BL21 pSarRare *E. coli*. The primers we used are listed in Table S1, and further details about purification strategies and conditions can be found in the Supplemental Experimental Procedures.

Crystallization and Structure Determination

Native and selenomethionine-substituted crystals were grown at 18°C using the hanging drop vapor diffusion method. Purified Kti13 protein in gel filtration buffer was concentrated to 10 mg/ml and combined with equal volume of 100 mM HEPES (pH 7.5) and 6% polyethylene glycol 3350. Crystals grew until day 7, were cryoprotected with 25% glycerol, and subsequently flash frozen in liquid nitrogen. Purified Kti11/Kti13 fusion protein in gel filtration buffer was concentrated to 10 mg/ml and combined with an equal volume of 100 mM Tris (pH 7.4–8.4) and 2 M Li_2SO_4. Crystals grew until day 3, were cryoprotected with 20% glycerol, and subsequently flash frozen in liquid nitrogen. A selenomethionine data set for Kti13 was collected at European Synchrotron Radiation Facility (ESRF) beamline ID14-4 on a Q315r ADSC detector. The Kti13 selenomethionine crystals diffracted to higher resolution than the native crystals, and the selenomethionine data set was therefore used for the refinement (Table 1). Native data sets for Kti13-$(GS)_5$-Kti11 were collected at the PETRAIII beamline P14 on a PILATUS 6M-F detector. Details about crystallographic software used for data processing, structure determination, and refinement can be found in the Supplemental Experimental Procedures.

ITC Measurements

ITC was performed with a VP-ITC calorimeter (Microcal). To measure the Kti11 Kti13 interaction, protein samples were dialyzed extensively against ITC buffer (20 mM Tris-HCl [pH 7.5], 125 mM NaCl, and 2 mM β-mercaptoethanol). Protein concentration in the cell was 10 μM and 100 μM in the injection syringe. The data were analyzed using Origin software (GE Healthcare).

NMR Analyses

All the NMR spectra were recorded on a Bruker 800 MHz Avance III spectrometer equipped with a CP-TCI cryoprobe at 25°C, and ^{1}H-^{15}N correlations were acquired by 2D fast HSQC. Previously reported zinc-bound Kti11 assignments (Sun et al., 2005) were used for further NMR analysis. A titration experiment was carried out by varying Kti13 from 5 to 100 μM, while keeping the Kti11 concentration constant at 50 μM. A complex of 50:15 Kti11:Kti13 was analyzed in detail. The NMR titration experiment was carried out in 20 mM Tris, 150 mM NaCl, 5 mM dithiothreitol (DTT) (pH 7.5), and 10% D_2O.

In Vitro Interaction Assays

We incubated 20 μg of GST-tagged Kti11 or Kti11 mutants and equal amounts of untagged Kti13 protein or mutants thereof overnight at 4°C with glutathione Sepharose in 20 mM Tris (pH 7.5), 150 mM NaCl, 5 mM DTT, and 0.1% Tween 20. The beads were washed five times with incubation buffer and subsequently resuspended in SDS loading buffer. Inputs and bound proteins were separated using denaturing SDS-PAGE and visualized using Coomassie blue stain.

Strains and Media

All *S. cerevisiae* strains used are listed in Table S2. Yeast strains were grown in rich media (0.8% yeast extract, 2% peptone) containing 2% glucose or 2% galactose or on minimal growth media. Solid medium was prepared by adding agar to 2% (w/v). Details of yeast manipulations including ^{55}Fe incorporation are indicated in the Supplemental Experimental Procedures.

In Vivo Interaction Assays

We added 100 μl of protein A Sepharose (PAS)-coupled α-HA primary antibody (for preparation protocol, see Supplemental Experimental Procedures) to the obtained yeast raw extracts. The mixture was then incubated on a shaker for 60 min at 4°C. Thereafter, the mixture was centrifuged at 1,000 rpm at 4°C for 1 min, and the supernatant was discarded. The PAS-coupled α-HA antibody pellet was washed three times with 1 ml of B60 buffer and centrifuged at 1,000 rpm for 1 min at 4°C. The PAS-coupled antibody pellet was resuspended in SDS buffer (10% SDS) and incubated at room temperature for 10 min. The suspension was centrifuged through a PCR-filter tip, and the flowthrough was analyzed by SDS-PAGE and western blotting.

Phenotypical Analyses of Mutants

To analyze the function of mutated *kti11* and *kti13* alleles, the γ-toxin or diphtheria toxin sensitivity was assayed as described previously (Frohloff et al., 2001; Mattheakis et al., 1992). Responses of yeast cells to intracellular expression of zymocin's lethal tRNase γ-toxin subunit involved the galactose-inducible *GAL1*-γ-toxin expression plasmid pHMS14. Sensitivity or resistance against diphtheria toxin was analyzed by using the intracellular expression plasmid pLMY101 (*URA3* marker) that was a kind gift of R. John Collier

(Harvard Medical School). pLMY101 carries the toxic diphtheria toxin fragment F2 under the galactose-inducible *GAL1*-promoter. Transformed strains were spotted in 10-fold serial cell dilutions on either 2% dextrose (repressing conditions)- or 2% galactose (inducing conditions)-containing plates and were incubated for 3 days at 30°C.

ACCESSION NUMBERS

The atomic coordinates and structure factors of Kti13 (PDB ID code 4D4Q) and iron-bound Kti11 in complex with Kti13 (PDB ID codes 4D4O and 4D4P) have been deposited with the European PDB.

SUPPLEMENTAL INFORMATION

Supplemental Information includes Supplemental Experimental Procedures, eight figures, and three tables can be found with this article online at http://dx.doi.org/10.1016/j.str.2014.11.008.

AUTHOR CONTRIBUTIONS

S.G. performed biochemical, biophysical, and crystallographic analyses. R.Z. performed coprecipitations and toxin assays. I.V. and A.-C.G. carried out the liposome binding assays. A.K. and J.B. performed NMR measurements. D.J.N., A.J.P., and R.L. determined in vivo iron levels. V.R. performed ITC measurements. S.G., K.D.B., and C.W.M. designed experiments, analyzed the data, and wrote the manuscript.

ACKNOWLEDGMENTS

We acknowledge support by the European Molecular Biology Laboratory (EMBL) Protein Expression and Purification Core Facility, the EMBL Advanced Light Microscopy Facility, the EMBL Heidelberg Crystallization Platform, and technical support by M. Stümpfig. We thank F. Baudin, T. Miller, and M. Jeske for comments on the manuscript. We also acknowledge access and support by the EMBL/ESRF Joint Structural Biology Group at ESRF beamlines and by the staff of EMBL Hamburg at PETRAIII beamline P14. This work was supported by the German Research Foundation (CRC [or SFB] 648 "Molecular mechanisms of information processing in plants" (TP B2 to K.D.B.). R.L. acknowledges generous support from Deutsche Forschungsgemeinschaft, von Behring-Röntgen Stiftung, LOEWE program of state Hessen, and Max-Planck Gesellschaft. C.W.M., S.G., I.V., and A.-C.G. acknowledge support by EMBL.

Received: October 9, 2014
Revised: November 11, 2014
Accepted: November 13, 2014
Published: December 24, 2014

REFERENCES

Abdel-Fattah, W., Scheidt, V., Uthman, S., Stark, M.J., and Schaffrath, R. (2013). Insights into diphthamide, key diphtheria toxin effector. Toxins (Basel) *5*, 958–968.

Bär, C., Zabel, R., Liu, S., Stark, M.J., and Schaffrath, R. (2008). A versatile partner of eukaryotic protein complexes that is involved in multiple biological processes: Kti11/Dph3. Mol. Microbiol. *69*, 1221–1233.

Bauer, F., Matsuyama, A., Candiracci, J., Dieu, M., Scheliga, J., Wolf, D.A., Yoshida, M., and Hermand, D. (2012). Translational control of cell division by Elongator. Cell Rep. *1*, 424–433.

Butler, A.R., White, J.H., Folawiyo, Y., Edlin, A., Gardiner, D., and Stark, M.J. (1994). Two Saccharomyces cerevisiae genes which control sensitivity to G1 arrest induced by Kluyveromyces lactis toxin. Mol. Cell. Biol. *14*, 6306–6316.

Cannarozzi, G., Schraudolph, N.N., Faty, M., von Rohr, P., Friberg, M.T., Roth, A.C., Gonnet, P., Gonnet, G., and Barral, Y. (2010). A role for codon order in translation dynamics. Cell *141*, 355–367.

Chen, C., Huang, B., Anderson, J.T., and Byström, A.S. (2011). Unexpected accumulation of ncm(5)U and ncm(5)S(2) (U) in a trm9 mutant suggests an additional step in the synthesis of mcm(5)U and mcm(5)S(2)U. PLoS ONE *6*, e20783.

Di Paolo, G., and De Camilli, P. (2006). Phosphoinositides in cell regulation and membrane dynamics. Nature *443*, 651–657.

Di Santo, R., Bandau, S., and Stark, M.J. (2014). A conserved and essential basic region mediates tRNA binding to the Elp1 subunit of the Saccharomyces cerevisiae Elongator complex. Mol. Microbiol. *92*, 1227–1242.

Dong, M., Su, X., Dzikovski, B., Dando, E.E., Zhu, X., Du, J., Freed, J.H., and Lin, H. (2014). Dph3 is an electron donor for Dph1-Dph2 in the first step of eukaryotic diphthamide biosynthesis. J. Am. Chem. Soc. *136*, 1754–1757.

Esberg, A., Huang, B., Johansson, M.J.O., and Byström, A.S. (2006). Elevated levels of two tRNA species bypass the requirement for elongator complex in transcription and exocytosis. Mol. Cell *24*, 139–148.

Frohloff, F., Fichtner, L., Jablonowski, D., Breunig, K.D., and Schaffrath, R. (2001). Saccharomyces cerevisiae Elongator mutations confer resistance to the Kluyveromyces lactis zymocin. EMBO J. *20*, 1993–2003.

Glatt, S., Létoquart, J., Faux, C., Taylor, N.M., Séraphin, B., and Müller, C.W. (2012a). The Elongator subcomplex Elp456 is a hexameric RecA-like ATPase. Nat. Struct. Mol. Biol. *19*, 314–320.

Glatt, S., Séraphin, B., and Müller, C.W. (2012b). Elongator: transcriptional or translational regulator? Transcription *3*, 273–276.

Huang, B., Johansson, M.J.O., and Byström, A.S. (2005). An early step in wobble uridine tRNA modification requires the Elongator complex. RNA *11*, 424–436.

Huang, B., Lu, J., and Byström, A.S. (2008). A genome-wide screen identifies genes required for formation of the wobble nucleoside 5-methoxycarbonylmethyl-2-thiouridine in Saccharomyces cerevisiae. RNA *14*, 2183–2194.

Jørgensen, R., Merrill, A.R., and Andersen, G.R. (2006). The life and death of translation elongation factor 2. Biochem. Soc. Trans. *34*, 1–6.

Jørgensen, R., Purdy, A.E., Fieldhouse, R.J., Kimber, M.S., Bartlett, D.H., and Merrill, A.R. (2008). Cholix toxin, a novel ADP-ribosylating factor from Vibrio cholerae. J. Biol. Chem. *283*, 10671–10678.

Karplus, P.A., and Diederichs, K. (2012). Linking crystallographic model and data quality. Science *336*, 1030–1033.

Kirkpatrick, D., and Solomon, F. (1994). Overexpression of yeast homologs of the mammalian checkpoint gene RCC1 suppresses the class of alpha-tubulin mutations that arrest with excess microtubules. Genetics *137*, 381–392.

Kishida, M., Tokunaga, M., Katayose, Y., Yajima, H., Kawamura-Watabe, A., and Hishinuma, F. (1996). Isolation and genetic characterization of pGKL killer-insensitive mutants (iki) from Saccharomyces cerevisiae. Biosci. Biotechnol. Biochem. *60*, 798–801.

Laxman, S., Sutter, B.M., Wu, X., Kumar, S., Guo, X., Trudgian, D.C., Mirzaei, H., and Tu, B.P. (2013). Sulfur amino acids regulate translational capacity and metabolic homeostasis through modulation of tRNA thiolation. Cell *154*, 416–429.

Liu, S., and Leppla, S.H. (2003). Retroviral insertional mutagenesis identifies a small protein required for synthesis of diphthamide, the target of bacterial ADP-ribosylating toxins. Mol. Cell *12*, 603–613.

Lu, J., Huang, B., Esberg, A., Johansson, M.J., and Byström, A.S. (2005). The Kluyveromyces lactis gamma-toxin targets tRNA anticodons. RNA *11*, 1648–1654.

Mattheakis, L.C., Shen, W.H., and Collier, R.J. (1992). DPH5, a methyltransferase gene required for diphthamide biosynthesis in Saccharomyces cerevisiae. Mol. Cell. Biol. *12*, 4026–4037.

Mehlgarten, C., and Schaffrath, R. (2003). Mutant casein kinase I (Hrr25p/Kti14p) abrogates the G1 cell cycle arrest induced by Kluyveromyces lactiszymocin in budding yeast. Mol. Genet. Genomics *269*, 188–196.

Novoa, E.M., Pavon-Eternod, M., Pan, T., and Ribas de Pouplana, L. (2012). A role for tRNA modifications in genome structure and codon usage. Cell *149*, 202–213.

Otero, G., Fellows, J., Li, Y., de Bizemont, T., Dirac, A.M.G., Gustafsson, C.M., Erdjument-Bromage, H., Tempst, P., and Svejstrup, J.Q. (1999). Elongator, a

multisubunit component of a novel RNA polymerase II holoenzyme for transcriptional elongation. Mol. Cell *3*, 109–118.

Pappenheimer, A.M., Jr. (1977). Diphtheria toxin. Annu. Rev. Biochem. *46*, 69–94.

Paraskevopoulou, C., Fairhurst, S.A., Lowe, D.J., Brick, P., and Onesti, S. (2006). The Elongator subunit Elp3 contains a Fe4S4 cluster and binds S-adenosylmethionine. Mol. Microbiol. *59*, 795–806.

Proudfoot, M., Sanders, S.A., Singer, A., Zhang, R., Brown, G., Binkowski, A., Xu, L., Lukin, J.A., Murzin, A.G., Joachimiak, A., et al. (2008). Biochemical and structural characterization of a novel family of cystathionine beta-synthase domain proteins fused to a Zn ribbon-like domain. J. Mol. Biol. *375*, 301–315.

Reddy Chichili, V.P., Kumar, V., and Sivaraman, J. (2013). Linkers in the structural biology of protein-protein interactions. Protein Sci. *22*, 153–167.

Rezgui, V.A., Tyagi, K., Ranjan, N., Konevega, A.L., Mittelstaet, J., Rodnina, M.V., Peter, M., and Pedrioli, P.G. (2013). tRNA tKUUU, tQUUG, and tEUUC wobble position modifications fine-tune protein translation by promoting ribosome A-site binding. Proc. Natl. Acad. Sci. USA *110*, 12289–12294.

Saliba, A.E., Vonkova, I., Ceschia, S., Findlay, G.M., Maeda, K., Tischer, C., Deghou, S., van Noort, V., Bork, P., Pawson, T., et al. (2014). A quantitative liposome microarray to systematically characterize protein-lipid interactions. Nat. Methods *11*, 47–50.

Selvadurai, K., Wang, P., Seimetz, J., and Huang, R.H. (2014). Archaeal Elp3 catalyzes tRNA wobble uridine modification at C5 via a radical mechanism. Nat. Chem. Biol. *10*, 810–812.

Sjölinder, M., Uhlmann, J., and Ponstingl, H. (2004). Characterisation of an evolutionary conserved protein interacting with the putative guanine nucleotide exchange factor DelGEF and modulating secretion. Exp. Cell Res. *294*, 68–76.

Stilger, K.L., and Sullivan, W.J., Jr. (2013). Elongator protein 3 (Elp3) lysine acetyltransferase is a tail-anchored mitochondrial protein in Toxoplasma gondii. J. Biol. Chem. *288*, 25318–25329.

Stirnimann, C.U., Petsalaki, E., Russell, R.B., and Müller, C.W. (2010). WD40 proteins propel cellular networks. Trends Biochem. Sci. *35*, 565–574.

Sun, J., Zhang, J., Wu, F., Xu, C., Li, S., Zhao, W., Wu, Z., Wu, J., Zhou, C.Z., and Shi, Y. (2005). Solution structure of Kti11p from Saccharomyces cerevisiae reveals a novel zinc-binding module. Biochemistry *44*, 8801–8809.

Tuller, T., Carmi, A., Vestsigian, K., Navon, S., Dorfan, Y., Zaborske, J., Pan, T., Dahan, O., Furman, I., and Pilpel, Y. (2010). An evolutionarily conserved mechanism for controlling the efficiency of protein translation. Cell *141*, 344–354.

Uhlmann, J., Wiemann, S., and Ponstingl, H. (1999). DelGEF, an RCC1-related protein encoded by a gene on chromosome 11p14 critical for two forms of hereditary deafness. FEBS Lett. *460*, 153–160.

Zabel, R., Bär, C., Mehlgarten, C., and Schaffrath, R. (2008). Yeast alpha-tubulin suppressor Ats1/Kti13 relates to the Elongator complex and interacts with Elongator partner protein Kti11. Mol. Microbiol. *69*, 175–187.

Zhang, Y., Liu, S., Lajoie, G., and Merrill, A.R. (2008). The role of the diphthamide-containing loop within eukaryotic elongation factor 2 in ADP-ribosylation by Pseudomonas aeruginosa exotoxin A. Biochem. J. *413*, 163–174.

Zhang, Y., Zhu, X., Torelli, A.T., Lee, M., Dzikovski, B., Koralewski, R.M., Wang, E., Freed, J., Krebs, C., Ealick, S.E., and Lin, H. (2010). Diphthamide biosynthesis requires an organic radical generated by an iron-sulphur enzyme. Nature *465*, 891–896.

